Journal of Controlled Release 325 (2020) 121–134

Contents lists available at ScienceDirect

Journal of Controlled Release

journal homepage: www.elsevier.com/locate/jconrel

Monograph

Ultrasound-mediated delivery enhances therapeutic efficacy of MMP sensitive liposomes

Marieke Olsman[a,*], Viktoria Sereti[b], Kristine Andreassen[a], Sofie Snipstad[a,c,f], Annemieke van Wamel[a], Rasmus Eliasen[b], Sigrid Berg[d,e,f], Andrew J. Urquhart[b], Thomas L. Andresen[b], Catharina de Lange Davies[a]

[a] Department of Physics, Norwegian University of Science and Technology, Trondheim, Norway
[b] Department of Health Technology, Center for Nanomedicine and Theranostics, Technical University Denmark, DTU Healthtech, Lyngby, Denmark
[c] Department of Biotechnology and Nanomedicine, SINTEF Industry, Trondheim, Norway
[d] Department of Circulation and Medical Imaging, Norwegian University of Science and Technology, Trondheim, Norway
[e] Department of Health Research, SINTEF Digital, Trondheim, Norway
[f] Cancer Clinic, St. Olavs Hospital, Trondheim, Norway

ARTICLE INFO

Keywords:
Drug delivery system
Ultrasound-mediated delivery
MMP sensitive liposomes
Doxorubicin
Sonopermeation

ABSTRACT

To improve therapeutic efficacy of nanocarrier drug delivery systems, it is essential to improve their uptake and penetration in tumour tissue, enhance cellular uptake and ensure efficient drug release at the tumour site. Here we introduce a tumour targeting drug delivery system based on the ultrasound-mediated delivery of enzyme sensitive liposomes. These enzyme sensitive liposomes are coated with cleavable poly(ethylene glycol) (PEG) which will be cleaved by two members of the enzyme matrix metalloproteinase family (MMP-2 and MMP-9). Cleavage of the PEG coat can increase cellular uptake and will destabilize the liposomal membrane which can result in accelerated drug release. The main aim of the work was to study the effect of focused ultrasound and microbubbles on the delivery and therapeutic efficacy of the MMP sensitive liposome. The performance of the MMP sensitive liposome was compared to a non-MMP sensitive version and Doxil-like liposomes. *In vitro,* the cellular uptake and cytotoxicity of the liposomes were studied, while *in vivo* the effect of ultrasound and microbubbles on the tumour accumulation, biodistribution, microdistribution, and therapeutic efficacy were investigated. For all tested liposomes, ultrasound and microbubble treatment resulted in an improved tumour accumulation, increased extravasation, and increased penetration of the liposomes from blood vessels into the extracellular matrix. Surprisingly, penetration depth was independent of the ultrasound intensity used. Ultrasound-mediated delivery of free doxorubicin and the Doxil-like and MMP sensitive liposome resulted in a significant reduction in tumour volume 28 days post the first treatment and increased median survival. The MMP sensitive liposome showed better therapeutic efficacy than the non-MMP sensitive version indicating that cleaving the PEG-layer is important. However, the Doxil-like liposome outcompeted the MMP and non-MMP sensitive liposome, both with and without the use of ultrasound and microbubbles.

1. Introduction

Successful treatment of cancer remains a challenge for many solid tumour types. Conventional chemotherapy is used alone or in combination with other treatment modalities and is based on systemic administration of drugs which often lacks cancer specificity, causing severe side-effects. Furthermore, because of high accumulation in healthy tissue and fast clearance rate of the small drug molecules, only a small fraction of the injected dose (0.001–0.01%) reaches the tumour site [1,2]. Therefore, new strategies are needed to obtain successful therapeutic response.

Drug loaded nanoparticles (NPs) have shown great potential as a more specific anti-tumour treatment being able to exploit the enhanced permeability and retention (EPR) effect in cancerous tissue and thereby improving the delivery of drugs to tumours and reducing toxic effects towards normal tissue [3,4]. Tumour tissue lacks lymphatic drainage and due to uncontrolled growth of tumours, endothelial cells are poorly aligned and have large fenestrations, resulting in leaky vasculature. These anatomical irregularities result in leakage and accumulation of components from the blood plasma into tumour tissue, which makes the

* Corresponding author.
E-mail address: marieke.olsman@ntnu.no (M. Olsman).

https://doi.org/10.1016/j.jconrel.2020.06.024
Received 10 February 2020; Received in revised form 18 June 2020; Accepted 22 June 2020
Available online 02 July 2020

EPR an interesting target for a more tumour specific therapy strategy [3,5]. NPs have numerous other advantages over conventional therapeutics such as less accumulation in healthy tissue and the possibility for actively targeted delivery by adding targeting ligands to the NP surface, in addition to protecting the drug from premature degradation, reviving potentially poorly soluble drugs, controlled and sustained drug release, and different pharmacokinetics and biodistribution compared to small molecule drugs [6]. However, despite these promising features, their therapeutic effect has been limited, partly by inadequate delivery due to the heterogeneous EPR-effect, dense extracellular matrix, and high interstitial fluid pressure in tumours [7–10].

Several preclinical studies have shown that ultrasound in combination with microbubbles improves the delivery, intratumoural distribution and therapeutic efficacy of drug loaded NPs in tumours [11–16]. The improved therapeutic efficacy of chemotherapeutics after ultrasound-mediated delivery has also been demonstrated in patients with non-resectable pancreatic tumours and patients suffering from glioblastoma [17,18]. In the acoustic field, the microbubbles expand and compress during the low and high pressure phases, respectively. This cavitation behaviour is known to increase the vascular permeability since the oscillating and collapsing microbubbles form mechanical stresses on the blood vessel wall which can create both transient and permanent pores or even more extensive vascular damage [19–21]. Furthermore, it has been shown that the use of focused ultrasound in combination with microbubbles can enhance endocytosis *in vitro* [19,22]. All these ultrasound-mediated effects, also known as sonopermeation, will increase vascular permeability and thereby increase extravasation and potentially improve penetration through the extracellular matrix which could result in enhanced accumulation and distribution of NPs and drug in tumour tissue [23].

Several NP-based drug delivery systems have been developed including polymeric, liposomal, viral and inorganic NPs [6]. These NPs are often coated with polyethylene glycol (PEG) to shield them from the immune system and thereby extending their circulation half-life significantly compared to non-PEGylated NPs and small drug molecules, resulting in an increased accumulation in tumour tissue [24]. In addition, PEGylation prevents aggregation of the NPs, and can have a charge shielding effect resulting in a more neutral charge of the NP, which may improve penetration through the extracellular matrix due to reduced electrostatic interactions with extracellular matrix components [25–27]. However, the presence of PEG on the surface of the NPs will also affect the NP-cell interaction, resulting in reduced cellular uptake and thereby potentially reducing the therapeutic efficacy [28,29].

To improve therapeutic outcome of current drug delivery systems, it is essential to improve the delivery of drug carriers to and throughout tumour tissue, enhance cellular uptake and ensure secure and efficient drug release at the tumour site. In the present work, we introduce a dual tumour targeting drug delivery system based on ultrasound-mediated delivery of matrix metalloproteinase (MMP) sensitive liposomes coated with PEG. Once delivered to the extracellular matrix of the tumour, the PEG coat will be cleaved by two members of the enzyme MMP family (MMP-2 and MMP-9) which are overexpressed in several cancer types [30]. The cleaving is expected to improve the interaction between liposomes and tumour cells compared to PEGylated liposomes [28,29]. Furthermore, removal of the PEG coating can result in accelerated drug release [29]. Based on the MMP sensitive liposome characteristics and the potentially improved delivery to the tumour site using ultrasound in the presence of microbubbles, it is hypothesized that this combination will enhance therapeutic efficacy.

The main aim of the work was to study the effect of focused ultrasound in combination with microbubbles on the delivery and therapeutic efficacy of the MMP sensitive liposome. The performance of the MMP sensitive liposome (Cleavable) was compared to a non-MMP sensitive version (NonCleavable) and a liposomal formulation the same as the clinically used formulation Doxil®/Caelyx® (Doxil-like). First, cellular uptake and cytotoxicity were studied *in vitro* by flow cytometry and a cell viability assay, respectively. Secondly, the effect of different ultrasound settings on liposome uptake in tumours and normal organs in mice was studied using a small animal optical imager, and the effect on microdistribution in tumours was evaluated with confocal laser scanning microscopy. Thirdly, the therapeutic efficacy of the drug loaded liposomes was evaluated by measuring the growth of subcutaneous tumours.

2. Material and methods

2.1. Peptide synthesis

The PEGylated cleavable lipopeptide (PCL) was synthesized as follows: The peptide H-Gly-Trp(Boc)-Ile-Pro-Val-Ser(tBu)-Leu-Arg-(Pbf)-Ser(tBu)-Gly-Glu(tBu)-Glu(tBu)-Glu(tBu)-Glu(tBu)-PEG_{2000} was synthesized on an Initiator Alstra peptide synthesizer (Biotage, Sweden) using a TentaGel PAP_{2000} resin. The resin was swelled in dichloromethane (DCM) for 1 hour. In general, couplings were carried out for 5 minutes at 75 °C using 4 equiv. amino acid, 3.92 equiv. HATU and 8 equiv. 2,4,6-collidine in N,N-Dimethylmethanamide (DMF). Ile and Leu were coupled twice to ensure conversion. The second coupling was carried out for 30 minutes at room temperature. Also, Arg was coupled for 30 minutes at room temperature. Ile, Val and Leu were coupled in N-methylpyrrolidone (NMP). Fmoc deprotection was performed using 20% piperidine in DMF for 10 minutes. The peptide was cleaved for 3 hours using 95:2.5:2.5 trifluoroacetic acid (TFA)/triisopropyl silane/water after which the cleavage solvent was removed under reduced pressure and the peptide precipitated in diethyl ether. The cleaved peptide was dissolved in 500:500:1 water/acetonitrile/triethylamine (TEA) and lyophilized. The peptide was hereafter dissolved in NMP and dried over molecular sieves in 3 mM concentration. 1.2 equiv. cholesteryl chloroformate and 20 equiv. diisopropylethylamine were added to the dissolved peptide and the solution was stirred. After 30 min the concentration was diluted to 10% NMP with water and purified using semipreparative high performance liquid chromatography (HPLC), which was operated using a Waters 600 pump and controller, a Waters 2489 UV/Vis detector and a Waters XTerra C18 5 μm column (30 × 250 mm). For lipopeptide elution, the following eluents were used: Eluent (A) 5% acetonitrile, 0.1% TEA in water, Eluent (B) 0.1% TEA in acetonitrile. A linear gradient was used for elution of the lipopeptide as a narrow peak with retention time (Rt) from 18-20 min was obtained. The lipopeptide was lyophilized to give a white powder. The purity of the compound was monitored by analytical HPLC using a Waters XTerra C8 (4.6 × 150 mm) column. Eluent (A) was 5% acetonitrile, 0.1% TFA and Eluent (B) 0.1% TFA in acetonitrile. A linear gradient from 0 to 100% eluent (B) over 15 min with flow rate 1 ml/min was used. The purity was >96% and Rt 11.8 min. Molecular weight was confirmed by use of MALDI-TOF MS (Bruker Reflex, Bruker Daltonics, USA) observed ($M+H^+$) 3983.9.

2.2. Liposome formulation and characterization

1-palmitoyl-2-oleoyl-glycero-3-phosphocholine (POPC) and ovine cholesterol (Chol) were purchased from Avanti Polar Lipids Inc. (USA). Methoxy(polyethylene glycol)-2000-Cholesterol (mPEG2000-Chol) was from Creative PEGWorks (USA). Stealth premix consisting of hydrogenated Soy-L-α-phosphatidylcholine (HSPC), hydrogenated 1,2-distearoyl-sn-glycero-3-phosphoethanolamine-N-[methoxy(polyethylene glycol)-2000] (mPEG2000-DSPE) and cholesterol in a weight ratio of 3:1:1: was purchased from Lipoid GmbH (Germany). To fluorescently label the liposomes, 1,2-dioleoyl-*sn*-glycero-3-phospho-ethanolamine-Atto488 (DOPE-Atto488) and 1,2-dipalmitoyl-*sn*-glycero-3-phosphoethanolamine-Atto700 (DPPE-Atto700) were used (ATTO-TEC GmbH, Germany). The PEGylated cleavable lipopeptide was fabricated in house as described in the previous section.

Liposomes were prepared using the molar compositions outlined in

Table 1
Molar compositions [%] of the three different liposomes.

	Fluorophore labelled liposomes			Drug loaded liposomes		
	Doxil-like	**NonCleavable**	**Cleavable**	**Doxil-like**	**NonCleavable**	**Cleavable**
POPC		59.6	59.6		60	60
HSPC	56.2			56.5		
Chol	38.1	35	35	38.2	35	35
MPEG2000-DSPE	5.3			5.3		
MPEG2000-CHOL		5			5	
PCL			5			5
DOPE-Atto488	0.2	0.2	0.2			
DPPE-Atto700	0.2	0.2	0.2			

***Abbreviations*:** POPC – 1-palmitoyl-2-oleoyl-*sn*-glycero-3-phosphocoline, HSPC – Hydrogenated soy 3-phosphocoline, CHOL – Cholesterol, DSPE – 1,2-Distearoyl-*sn*-glycero-3phosphoetanolamine, PEG2k – Polyethylene glycol, PCL – PEGylated cleavable lipopeptide, DOPE-Atto488 – 1,2-Dioleoyl-*sn*-glycero-3-phosphoethanolamine-Atto488, DPPE-Atto700 – 1,2-Dipalmitoyl-*sn*-glycero-3-phosphoethanolamine-Atto700.

Table 1. Appropriate amounts of the phospholipids were dissolved in a mixture of t-Butanol:water (9:1), which was snap-frozen in liquid nitrogen and lyophilized overnight. The following day the thin lipid layer was hydrated in a 10 mM HEPES 140 mM NaCl buffer or 250 mM ammonium sulfate buffer (fluorophore labelled liposomes or doxorubicin loaded liposomes respectively) and extruded by passing the multilamellar vesicles through 100 nm polycarbonate filters to form unilamellar vesicles. The temperature was kept at 40 °C for unsaturated formulations (NonCleavable and Cleavable) and 65 °C for saturated formulations (Doxil-like) throughout the hydration and extrusion process. Liposomes hydrated with ammonium sulfate were dialyzed using Slize-A-Lyzer cassettes (ThermoFisher, USA), pore size 10 kD versus a 10 mM HEPES 140 mM NaCl buffer. Subsequently, the dialyzed liposomes were remote loaded with doxorubicin HCl (Lianyungang Guivuan Chempharm Co., China) for 3 hours at 45 °C (unsaturated liposomes) or 60 °C (saturated liposomes), at a drug-to-lipid ratio of 1:5. Unencapsulated doxorubicin was removed by dialyzing the liposomes using Slide-A-Lyzer dialysis cassettes (MWCO 10kD) versus HEPES saline buffer (10 mM HEPES, 140 mM NaCl, pH7.4). The PEG cleavable lipopeptide was post inserted to the corresponding formulations at 40 °C for 45 min.

The phosphor content of the liposomes was quantified using Inductive Coupled Plasma Mass Spectroscopy (ICP-MS), employing gallium as internal standard, while the doxorubicin content of the liposomes was quantified spectrophotometrically by measuring sample absorption at 496 nm (Tecan Spark plate reader, Tecan Trading, Switzerland). The hydrodynamic radius, polydispersity index (PDI) and zeta potential of the liposomes were investigated using a Zetasizer ZS (Malvern Panalytical Ltd., UK). The liposomes were diluted to 100 μM using HEPES saline buffer (10 mM HEPES, 140 mM NaCl) for DLS measurements and 10 mM HEPES 5% w/v glucose for zeta potential measurements.

Phospholipids labelled with Atto488 and Atto700 (see Table 1) were incorporated in the liposomes to measure the microdistribution and tissue uptake of liposomes, respectively. The fluorescence intensity of the three liposomes was compared by measuring the fluorescence intensity of Atto488 and Atto700 in dilution series of the liposomes using a spectrofluorometer (SpectraMax i3x, Molecular Devices, USA) and a small animal optical imager (Pearl Impulse imager, LI-COR Biosciences Ltd., USA). Results from the dilution series measured by the small animal optical imager were compared to *in vivo* fluorescence intensity measurements. For the spectrofluorometer experiments, the liposome solutions were excited with 480 ± 9 nm and 680 ± 9 nm and emissions were detected at 505 ± 20 nm and 705 ± 20 nm, for respectively Atto488 and Atto700. For experiments with the small animal optical imager, the Atto700-liposomal solutions were excited with 685 nm and fluorescence emission was detected at 720 nm.

2.3. In vitro cleavage of the MMP sensitive liposomes

The protease thermolysin has the same substrate specificity as MMP-2 and MMP-9, and is therefore suitable for cleavage of the liposomes *in vitro* [31]. 20 μl of liposomes were mixed with 6 μg/ml thermolysin in 180 μl of enzyme activation buffer which consists of HEPES-buffered saline (50 mM HEPES, 100 mM NaCl, pH 7.4) supplemented with 1 mM $CaCL_2$ and 2 μM $ZnCl_2$. All chemicals were purchased at Sigma-Aldrich (USA). The cleavage was performed over night at 37 °C.

2.4. Cell culture

Prostate adenocarcinoma cells (PC3, ATCC, USA) were cultured in Dulbecco's modified Eagle medium (Sigma-Aldrich, USA) with 10% fetal bovine serum (Sigma-Aldrich, USA). Cells were kept at 37 °C and 5% CO_2 and maintained in exponential growth. 1% penicillin/streptomycin (Sigma-Aldrich, USA) was added to the growth medium of cells implanted in mice and the *in vitro* cytotoxicity study.

2.5. Cellular uptake of liposomes

50 000 PC3 cells/well were seeded in 24-well plates (VWR, USA). Seventy-two hours post seeding, cells were incubated with 50 μg/ml of doxorubicin loaded liposomes (Doxil-like, NonCleavable, Cleavable) for 4 hours at 37 °C and 5% CO_2 before washing 3 times with PBS, trypsinizing (Sigma-Aldrich, USA) and placing the cell suspension on ice until flow cytometry analysis. To study the effect of cleavage of the Cleavable liposome on the cellular uptake, both the intact and cleaved version (thermolysin treated) of the Cleavable liposome were included. To evaluate if any dye leakage (doxorubicin) occurred, cells were incubated with 50 μg/ml of doxorubicin loaded liposome solution for 4 hours at 4 °C. No endocytosis is expected at this temperature such that stained cells are most likely stained due to free drug [32].

Liposomal uptake was evaluated by flow cytometry (Gallios, Beckman Coulter, USA). A 488 nm laser was used for excitation of doxorubicin and emission was detected at 585 ± 15 nm. Gating on the side versus forward scatter plot was applied to exclude dead cells, debris and cell aggregates. Kaluza Flow Cytometry analysis software v1.3 (Beckman Coulter, USA) was used to determine the percentage of fluorescent cells and mean fluorescence intensity corresponding to cellular uptake of liposomes.

2.6. In vitro cytotoxicity study

The metabolic assay based on AlamarBlue was used to measure cell viability. 10 000 PC3 cells/well were seeded in a black 96 well plate with transparent bottom (Corning Inc., Sigma-Aldrich, USA). Twenty-four hours after seeding, cells were incubated with either the drug loaded liposomes or free doxorubicin (Accord Healthcare, UK) for 24

hours at 37 °C with 5% CO_2. For both free and encapsulated doxorubicin, concentrations between 0.001 μg/ml and 100 μg/ml, were used. After treatment, cells were rinsed 3 times with growth medium. The growth medium was replaced by 100 μl of AlamarBlue (1:10 dilution in growth medium) (Thermo Fisher Scientific, USA) 24 hours later, and incubated for 3 hours. Fluorescence was measured with a spectrofluorometer (SpectraMax i3x, Molecular Devices, USA) with excitation at 560 nm and detection of emission at 590 nm. Cell viability was calculated by dividing the fluorescence intensity of the treated wells by the fluorescence intensity of wells with untreated cells. A four-parameter logistic curve was fitted to the datapoints with SigmaPlot (v14.0, Systat Software Inc., USA).

2.7. Animals and tumour inoculation

Female Balb/c nude mice (Janvier labs, France) were purchased at 8 weeks of age. Mice were housed in groups of 5 in individually ventilated cages under conditions free of specific pathogens at a 12-hour night/day cycle. Cages were kept in a controlled environment (20–23 °C, humidity of 50–60%) and the mice had free access to food and sterile water. They were fed RM1 expanded pellets (Special Diets Services, UK), and the cages were enriched with housing, nesting material and gnaw sticks. All experimental procedures were approved by the Norwegian Food Safety Authority.

Before tumour implantation, mice were anesthetized with 2–3% isoflurane. 50 μl of medium containing $3x10^6$ PC3 cells was slowly injected subcutaneously between the hip and the knee on the lateral side of the left hind leg. Tumours were measured with a calliper 3 times per week and the weight of the animals was closely monitored. Tumour volume was calculated by $l * w^2 * \frac{\pi}{6}$, where l and w are the length and width of the tumour, respectively.

Before ultrasound experiments, mice were anesthetized by a subcutaneous injection (0.1 ml/10 g of bodyweight) of fentanyl (0.05 mg/kg, Actavis Group, USA), medetomidine (0.5 mg/kg, Orion Pharma, Finland), midazolam (5 mg/kg, Accord Healthcare, UK) and water (2:1:2:5). Thereafter a catheter was placed in the lateral tail vein. In case needed, a subcutaneous injection (0.1 ml/10 g of body weight) of atipemazol (2.5 mg/kg, Orion Pharma, Finland), flumazenil (0.5 mg/kg, Fresenius Kab, USA) and water (1:1:8) was used as antidote. The mice received a subcutaneous injection of 0.5 ml saline before waking up to counteract the incurred dehydration. Body temperature was maintained by external heating and eyes were kept moist with Viscotears Liquid Gel (Alcon, USA). After treatment, the animals were placed in a recovery rack (28 °C) until the next morning to recover from the anaesthesia and avoid hypothermia. At the end of experiments, the anesthetized mice were euthanized by cervical dislocation.

2.8. Ultrasound set-up, microbubbles and passive cavitation detection

A custom-made single element focused transducer (Imasonic, France) with a centre frequency of 1.0 MHz was mounted on the bottom of a water tank (see Fig. 1). The transducer had a diameter of 50 mm and a focal distance of 125 mm. Signals were generated with a signal generator (33500B, Agilent Technologies, USA) and amplified with a 50 dB RF amplifier (2100L, E&I, USA).

Animals were placed on top of the lid of the tank and the tumour bearing leg was positioned through a circular hole in the lid and in the far field of the ultrasound transducer at a distance of approximately 190 mm. The 3 dB and 6 dB beam widths at 190 mm distance are 6 and 10 mm, respectively, thereby exposing the whole tumour. The waterside of the lid was covered with acoustic absorber material to avoid standing waves. To avoid hypothermia of the animal, water in the tank was heated to 32 °C and a heating lamp was placed above the mouse. Animals exposed to ultrasound received a 100 μl bolus injection of SonoVue™ microbubbles (Bracco Imaging, Italy) directly after an intravenous bolus injection of liposomes, after which ultrasound treatment was started within 5 seconds.

The *in vivo* cavitation behaviour of the SonoVue™ microbubbles was detected with a 5.0 MHz unfocused transducer (Harisonic, 0.75 inch diameter, 17-0512-P, Olympus, USA) which was placed in a custom-made holder in the corner of the tank facing the tumour leg. The detected backscatter signal was recorded by an oscilloscope (LeCroy WaveRunner 44Xs, LeCroy corporation, USA) with a sampling frequency of 100 MS/s and transferred to a PC for processing in Matlab (version R2018A, Mathworks Inc, USA). The frequency content of the signals was calculated and displayed real time, enabling visual inspection of an expected increase in harmonic signals (stable cavitation) and broadband level rise (inertial cavitation).

2.9. Ultrasound-mediated delivery of the three liposomes

Subcutaneous prostate cancer tumours were grown in 40 mice, and mice were included when the tumours had reached an average size of 200–300 mm^3. For each type of liposome, the animals were randomly divided into 3 treatment groups (Table 2).

Each animal received an 100 μl intravenous bolus injection of 6 mM of liposome solution. Mice exposed to ultrasound, received 100 μl of SonoVue™ microbubbles followed with 2 minutes of ultrasound with either a mechanical index (MI) of 0.4 or 0.8 (0.4 or 0.8 MPa peak negative pressure), with ultrasound pulses of 10 000 cycles and pulse repetition frequency of 0.5 Hz.

Three hours post injection of liposomes, functional blood vessels were stained by injecting 100 μl of lectin (*Ulex europaeus*-Atto 594 conjugate, Sigma-Aldrich, USA) which was allowed to circulate for 5 min before euthanizing the animal.

2.10. Tumour accumulation and biodistribution of liposomes – Small animal optical imager

Tumour accumulation of the liposomes was obtained by imaging animals with a small animal optical imager (Pearl Impulse imager, LI-COR Biosciences Ltd., USA) at different timepoints post treatment. The Atto700 dye in the liposomes was excited at 685 nm and emission was detected at 720 nm. In addition to the fluorescence image, a bright field

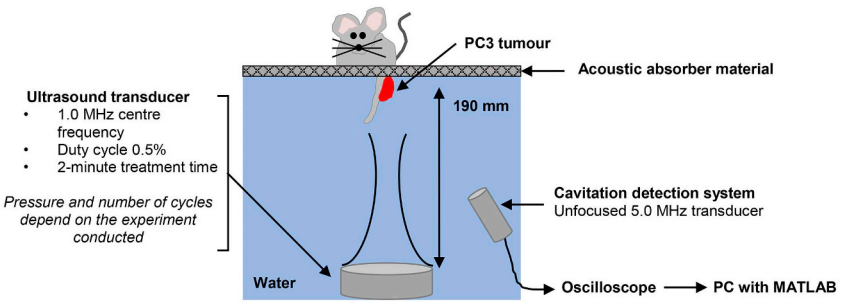

Fig. 1. Schematic illustration of the ultrasound set up.

Table 2
Treatment groups to study the effect of ultrasound and microbubbles on tumour accumulation, biodistribution and microdistribution of the three liposomes. (D = Doxil-like, NC = NonCleavable, C = Cleavable).

Group	Liposome	Mechanical index	Number of cycles	Pulse repetition frequency [Hz]	Treatment time [min]	Number of mice
1	D	–	–	–	–	3
2	D	0.4	10 000	0.5	2.0	5
3	D	0.8	10 000	0.5	2.0	5
4	NC	–	–	–	–	3
5	NC	0.4	10 000	0.5	2.0	5
6	NC	0.8	10 000	0.5	2.0	5
7	C	–	–	–	–	4
8	C	0.4	10 000	0.5	2.0	5
9	C	0.8	10 000	0.5	2.0	5

image of the animal was recorded. At each timepoint, a region of interest (ROI) around the tumour was drawn on the bright field image, transferred to the fluorescence image and the average fluorescence intensity of the ROI was obtained. The tumour fluorescence intensity as a function of time was normalized to the fluorescence intensity at t = 0 (first recorded image approximately 5 minutes after injection of the liposomes).

The biodistribution of NPs was obtained by excising the spleen, kidneys, liver, lungs, heart and tumour. Both a fluorescence and a bright field image of the organs were obtained. An ROI was drawn around each organ and the total fluorescence intensity was normalized by the wet weight of the organ or tumour. The fluorescence intensity per gram of tissue was plotted per liposome and treatment group. Fluorescence intensity values for the biodistribution were corrected based on the observed differences in fluorescence intensity of the Atto700 between the three liposomes.

2.11. Microdistribution – Confocal imaging of tumour sections

Excised tumours were cut along the coronal plane. One half was mounted with the cutting plane down on a piece of cork and covered with OCT Tissue Tek (Sakura, The Netherlands) before submerging the sample in liquid nitrogen and storing at −80 °C. The other half was fixed in 4% paraformaldehyde for histological evaluation.

Of the frozen tissue samples, the first 1000 μm was removed after which 4 sections of 25 μm thickness for confocal imaging and 1 section of 4 μm thickness for histological evaluation were taken. These 5 sections were made at 5 different levels in the tumour, separated by 300 μm.

Microdistribution of the liposomes was imaged by confocal laser scanning microscopy (CLSM). Prior to imaging, the section was thawed at room temperature, mounted with Vectashield containing DAPI (Vector Laboratories, USA), covered with a cover glass and sealed with nail polish. The DAPI staining was used to distinguish between tumour and healthy tissue. All sections were imaged with a Leica TCS SP8 confocal microscope equipped with a white light laser (Leica Microsystems, Germany) and a multiphoton laser (Chameleon Vision-S, Coherent, USA) and using a 40X/1.10 water objective. DAPI was excited with the multiphoton laser at 730 nm and emission was detected at 400–450 nm. Sequentially, the Atto488 in the liposomes and the Atto594 from the blood vessel staining were excited with a white light laser at 500 and 600 nm, respectively. Fluorescence of these two dyes was detected at 515–555 nm and 615–655 nm, respectively. An optical section of 4 μm was used and the laser intensity and detector gain were kept the same for all sections.

Sections were inspected through the ocular by viewing only the blood vessel channel and images were taken whenever stained blood vessels were found without knowing whether liposomes were present or not. From each treatment group, sections at three different levels from the tumour of three animals per treatment group were imaged resulting in 80–110 images per treatment group (approximately 7–14 images per section).

2.12. Microdistribution – Quantification of extravasation

Images taken with the CLSM (see Supplementary Fig. S1A) were processed and analysed in ImageJ and MATLAB (version R2018A, Mathworks Inc, USA). The blood vessel and liposome images were thresholded based on the ImageJ built-in threshold 'Triangle' (see Supplementary Fig. S1B). From the thresholded blood vessel channel, a distance map image was calculated in which the intensity of each pixel represents the distance of that specific pixel to the nearest blood vessel pixel in number of pixels (see Fig. S1C). This distance map image was multiplied pixel by pixel with the thresholded binary liposome image resulting in a distance map image for just the pixels representing extravascular liposomes (see Fig. S1D). From each image a histogram was created to assess the distance travelled by the liposomes and the distance travelled was converted from number of pixels to micrometre (1 pixel = 0.6 μm) (see Fig. S1E).

Several histograms showed small but clear peaks at distances far from the blood vessel wall. It is expected that these peaks are caused by liposomes from blood vessels that were above or below the imaged plane or blood vessels that were not functional at the time the lectin was circulating, and these peaks were excluded. Thereafter, the average number of pixels at each distance from the blood vessel of the whole dataset was calculated and plotted per liposome and treatment group.

2.13. Therapeutic efficacy study

Mice were included in the therapeutic efficacy study once the tumours had reached a size of 100–200 mm^3, 3–4 weeks after inoculation. A total of 55 mice were randomly distributed in the nine different treatment groups (see Table 3).

Untreated control animals received a sham saline injection of 200 μl. Mice getting treatment received a doxorubicin dose of 6 mg/kg by intravenously injecting either the doxorubicin loaded liposomes or the free drug doxorubicin (Doxorubicin Hydrochloride, Accord

Table 3
The nine treatment groups during the therapeutic efficacy study. (FUS = Focused ultrasound treatment in the presence of microbubbles).

	Abbreviation		Number of mice	
Treatment	**−FUS**	**+FUS**	**−FUS**	**+FUS**
Saline	Saline	–	7	–
Doxil-like	D	D + FUS	7	5
NonCleavable	NC	NC + FUS	6	6
Cleavable	C	C + FUS	5	6
Doxorubicin	DOX	DOX + FUS	6	7

Healthcare, UK). Groups not exposed to ultrasound and microbubbles (-FUS), received a 100 μl sham saline injection while groups exposed to ultrasound received 100 μl SonoVue™ microbubbles followed by an ultrasound treatment with an MI of 0.8 and pulses with 10 000 cycles (+FUS). Animals received this treatment once a week for three consecutive weeks (day 0, 7 and 14).

Tumour sizes were measured with a calliper three times a week and the weight of the animals was closely monitored. Mice were euthanized when the tumour length exceeded 15 mm. Animals that showed a reduced tumour growth with respect to the saline group for at least 7 consecutive days were defined as responders.

2.14. Statistical analysis

Statistical analysis on all datasets was performed with Sigmaplot (v14.0, Systat Software Inc., USA). Datasets were first tested for normality and equal variance with the Shapiro-Wilk test and Brown-Forsythe test, respectively. If the dataset passed for both tests, a t-test was performed to test for statistical significance between two treatment groups. Otherwise a Mann-Whitney rank sum test was used to assess statistical significance between datasets. A p-value smaller than 0.05 was considered to indicate statistical significance.

3. Results

3.1. Characterization of liposomes

Characteristics such as size, polydispersity index (PDI), zeta potential and loading of doxorubicin are shown in Table 4. A circulation half-life time of 2.9, 4.0 and 3.2 hours were observed for the Doxil-like, NonCleavable and Cleavable liposome, respectively (see Table S1 and Fig. S2). Different batches of the liposomes were used for the *in vitro* and *in vivo* experiments.

The effect of thermolysin on size, PDI and zeta potential of the three liposomes has been studied (Supplementary Fig. S3). Small differences in size or zeta potential between the liposomes were found.

The fluorescence intensity of the Atto700 dye were measured by the small animal optical imager of liposomes in solution and *in vivo* in the non-tumour bearing leg, and shown in Supplementary Fig. S4A and B, respectively. A large difference in fluorescence intensity between the three types of liposomes was observed. The NonCleavable liposomes showed fluorescence intensities that were approximately 3.7x and 1.9x higher than those of the Doxil-like and Cleavable liposomes, respectively. The differences observed in solution corresponded well with the *in vivo* data obtained 5 minutes after injection of the liposomes. The fluorescence intensity of the Atto488 and Atto700 was also measured with a spectrofluorometer (Supplementary Fig. S5) and corresponded to Fig. S4.

3.2. Cellular uptake and in vitro cytotoxicity of doxorubicin loaded liposomes

The uptake of the liposomes by PC3 cells after 4 hours of incubation at 37 °C was evaluated by flow cytometry and the results are shown in Fig. 2A. 90% of the cells had taken up the NonCleavable liposome, followed by the Cleavable and Doxil-like liposomes with 68% and 26% of cellular uptake, respectively. The mean fluorescence intensity of the cells incubated with liposomes increased by a factor of 3.9x to 5.5x with respect to untreated autofluorescence values (see Fig. 2B). Both the cellular uptake (%) and the mean fluorescence intensity increase were significantly different from autofluorescence and between the different liposomes. Incubating at 4 °C for 4 hours did not result in any cellular uptake of the liposomes while free drug doxorubicin showed clear uptake. This indicates that there was no free drug (doxorubicin) in the liposomal solutions (data not shown).

The *in vitro* toxicity of the three doxorubicin loaded liposomes and free doxorubicin are shown in Fig. 2C. A reduction in cell viability was observed for increasing concentrations of encapsulated and free drug. For most of the concentrations tested, the NonCleavable and Cleavable liposomes showed a similar effect on the cell viability as free doxorubicin. A higher concentration of the Doxil-like liposome was needed to reduce cell viability.

The effect of cleavage of the PEG-layer of the Cleavable liposome on the cellular uptake has been studied (Supplementary Fig. S6). The figure shows that the enzyme activation buffer without the enzyme added to the growth medium reduced the cellular uptake from 68% for the Cleavable liposome in just growth medium to 38%. Adding the enzyme thermolysin significantly increased the cellular uptake to 55%. A reduced cellular uptake of the NonCleavable liposome was observed after adding the activation buffer without the enzyme. Adding the enzyme had no effect on the cellular uptake. The cellular uptake of the Doxil-like was not affected by neither adding the buffer nor the buffer and the enzyme.

3.3. Ultrasound-mediated tumour accumulation of fluorophore labelled liposomes

The effect of ultrasound and microbubbles on tumour accumulation of the three fluorophore labelled liposomes is shown in Fig. 3. Ultrasound settings used were based on the previous obtained results showing large tumour accumulation of the liposomes using an MI of 0.8 with pulses of 10 000 cycles and intermediate tumour accumulation of

Table 4
The average diameter, ς-potential and PDI for the fluorophore labelled and doxorubicin loaded liposomes. Different batches of the liposomes were used for the *in vitro*, *in vivo* tumour accumulation and therapeutic efficacy study.

Doxorubicin Loaded - *Cellular uptake + cytotoxicity*	**Diameter [nm]**	**ς-potential [mV]**	**PDI**	**Dox to lipid ratio [μmol dox/μmol lipid]**
Doxil-like	128	−14.6 ± 0.9	0.063 ± 0.009	0.23
NonCleavable	123	−11.4 ± 0.4	0.054 ± 0.008	0.24
Cleavable	140	−17.6 ± 0.6	0.059 ± 0.025	0.24
Fluorophore Labelled - *Microdistribution + Biodistribution*				
Doxil-like	126	−13.4 ± 0.5	0.035 ± 0.007	-
NonCleavable	155	−3.8 ± 1.2	0.102 ± 0.020	-
Cleavable	160	−13.7 ± 1.2	0.044 ± 0.015	-
Doxorubicin Loaded - *Therapeutic efficacy study*				
Doxil-like	105	−5.4 ± 0.5	0.055 ± 0.019	0.20
NonCleavable	94	−5.5 ± 0.1	0.081 ± 0.007	0.24
Cleavable	127	−12.7 ± 0.2	0.068 ± 0.020	0.27

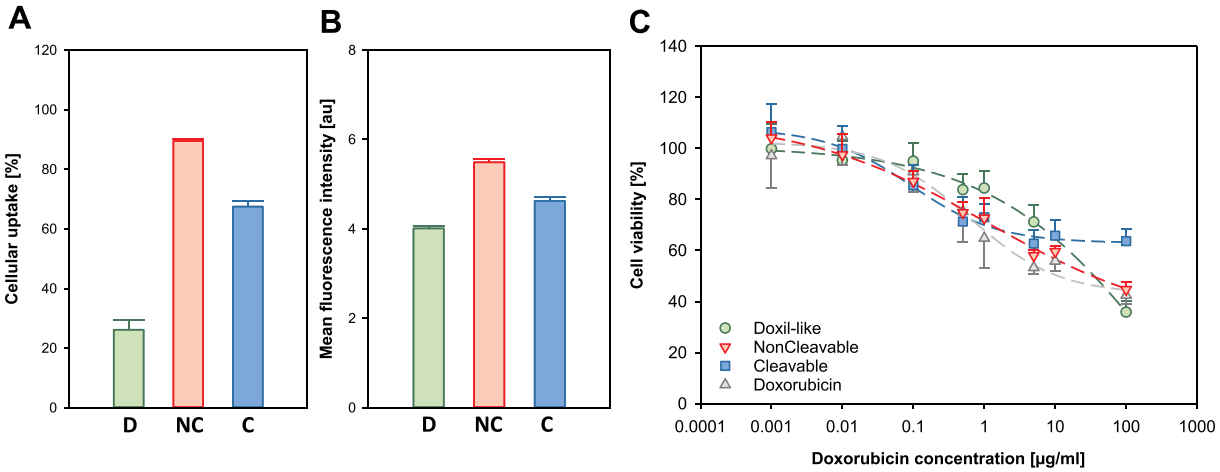

Fig. 2. (A) Cellular uptake of liposomes in percentage and (B) mean fluorescence intensity normalized to autofluorescence after 4 hours of incubation. Mean and standard deviation are based on the averages of n = 3 experiments (three replicates each). (D = Doxil-like, NC = NonCleavable, C = Cleavable) (C) Cytotoxicity of the drug loaded liposomes and free drug doxorubicin for PC3 cells after incubation of 24 hours at 37 °C and a recovery time of 24 hours before applying the AlamarBlue assay. A four-parameter logistic curve was fitted to the datapoints. Mean and standard deviation are based on the averages of n = 3 experiments (three replicates each).

the liposomes using MI = 0.4 with 10 000 cycles (Supplementary Fig. S7).

Representative images taken at t = 0 (approx. 5 minutes after treatment) and t = 3 hours post injection of the Cleavable liposomes with and without ultrasound treatment are shown in Fig. 3A. The fluorescence intensity relative to fluorescence intensity at t = 0 of the tumour ROI as function of time are shown in Fig. 3B–D. Ultrasound and microbubbles increased the tumour uptake of all liposomes, but to different extents. A statistically significant increase in relative fluorescence intensity could be observed at all timepoints (t > 0). All ultrasound-treated groups reached their maximum intensity at 0.5 hours post injection of the liposomes. The increase in relative fluorescence intensity was most profound for the NonCleavable liposome of which the groups treated with an MI of 0.4 and 0.8 reached average peak values of 1.7 and 2.2, respectively. The Doxil-like and Cleavable liposome responded similarly and the MI = 0.4 and MI = 0.8 ultrasound treatment groups reached a maximum relative fluorescence intensity of 1.2–1.3 and 1.5, respectively.

Three hours post injection, the tumour accumulation of all liposomes was reduced (Fig. 3D), but the ultrasound treated groups still had higher fluorescence intensity than the corresponding groups without ultrasound treatment (Only-LPs). Even though the NonCleavable liposome showed the highest increase of relative fluorescence intensity at 0.5 hours post injection, at 3 hours post injection, the relative fluorescence intensity values of the MI = 0.8 group differed minimally from the other two MI = 0.8 groups. The Only-LPs and MI = 0.4 group of the NonCleavable liposome showed lower values than the Doxil-like and Cleavable liposome. The relative fluorescence intensity readings of the groups treated with ultrasound in combination with the Doxil-like or Cleavable liposome reached similar values at 3 hours post injection and treatment. The decrease of fluorescence intensity over time is expected to be due to elimination of the liposomes from the circulation and by liposome clearance in the tumour.

3.4. Biodistribution of liposomes

Fig. 4 shows the biodistribution of the three liposomes in the different treatment groups. Fluorescence intensity per gram of tissue is displayed for the various organs and tumour. Here, the fluorescence intensity has been corrected based on fluorescence intensity differences of the Atto700 dye between the three different types of liposomes.

The Doxil-like and Cleavable liposome showed a similar biodistribution profile in the various organs, while the NonCleavable liposome showed lower fluorescence intensity values for most organs. Furthermore, highest fluorescence intensities for all three liposomes were observed in the lungs followed by the spleen, liver, kidneys and heart.

An increase in fluorescence intensity in the tumour could be observed when ultrasound and microbubbles were used in combination with the liposomes. The effect of ultrasound and microbubbles seemed to be minimal for the Doxil-like liposome. Only the MI = 0.8 group of the NonCleavable liposome showed a statistically significant increase with respect to the Only-LPs treatment group ($p < 0.05$). For most organs, ultrasound and microbubbles did not change the biodistribution profile. Only the MI = 0.4 group of the Doxil-like and NonCleavable liposome showed a significant reduction in fluorescence intensity with respect to the Only-LPs treatment group in the liver and kidneys, respectively ($p < 0.05$).

3.5. Microdistribution of liposomes

The microdistribution of liposomes was imaged by CLSM of frozen tumour sections. Representative images from a tumour in the control group and a tumour treated with MI = 0.8 ultrasound and microbubbles are shown in Fig. 5A-B, respectively. An increased prevalence of permeation of the liposomes into the extracellular matrix of the tumour can be observed.

A more quantitative analysis of the CLSM images revealed more details regarding the extravasation and distance travelled by the liposomes into the extracellular matrix of the tumour. From the CLSM images, the number of pixels representing extravasated liposomes was summed per image and plotted per treatment group and liposome as a boxplot (see Fig. 5C). The number of pixels representing extravascular liposomes increased when ultrasound and microbubbles were used. For all liposomes, the increase in number of pixels representing extravasated liposomes was minimal for the MI = 0.4 group but was more profound for the MI = 0.8 group. In case of the Doxil-like liposome, amount of extravasation in both ultrasound treatment groups was statistically significant with respect to the Only-LPs treatment group. This was only the case for the MI = 0.8 group of the NonCleavable and Cleavable liposome.

Comparing the three liposomes, mice treated with the Cleavable liposome showed higher number of pixels representing extravasated liposomes in both the Only-LPs treatment group and both ultrasound treatment groups than mice receiving the Doxil-like or NonCleavable liposome.

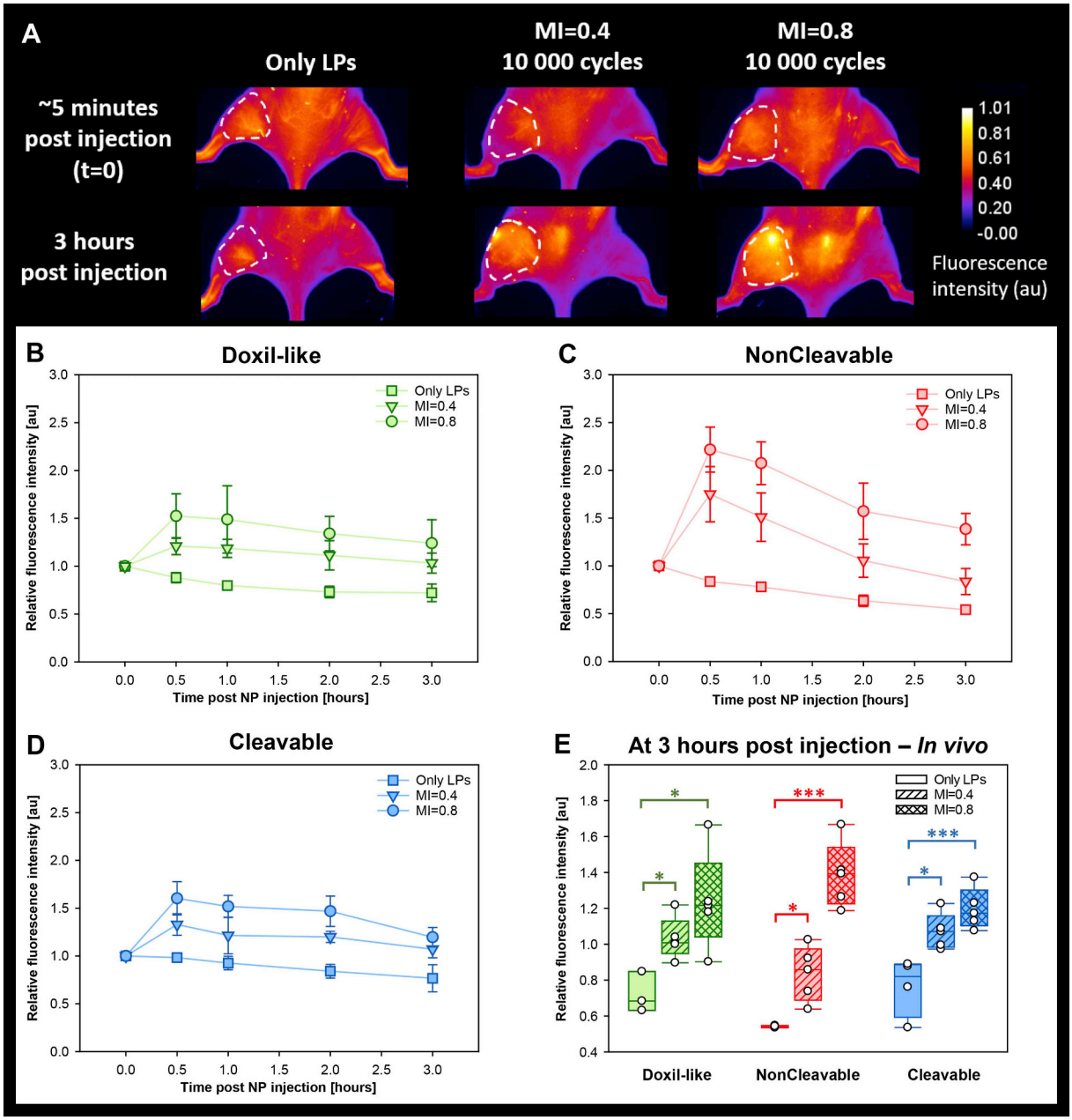

Fig. 3. (A) Representative images taken at t = 0 (~5 minutes) and 3 hours post injection of the liposomes of animals treated with and without ultrasound. White dashed line depicts the tumour ROI. (B-D) The mean relative fluorescence intensity of tumour ROI as function of time for the Doxil-like, NonCleavable and Cleavable liposome, respectively. Normalization was done relative to values at t = 0. Mean and standard deviation are based on 3–5 animals. (E) Boxplot of the *in vivo* mean relative fluorescence intensity in the tumour ROI at 3 hours post liposome injection. The circular symbols depict different animals. Statistically significance is indicated with asterisks (*p < 0.05, ***p < 0.001).

The effect of ultrasound and microbubbles on the displacement of liposomes from the blood vessels are shown in Fig. 5D–F for the Doxil-like, NonCleavable and Cleavable liposome, respectively. When ultrasound was used, liposomes were observed up to approximately 65 μm away from the blood vessel, independently of which MI and liposome were used. In the case of the Doxil-like and NonCleavable liposome, a doubling of distance travelled could be observed after exposure to ultrasound in the presence of microbubbles. The Cleavable liposomes seemed to extravasate and penetrate well without help of ultrasound and microbubbles compared to the Doxil-like and NonCleavable liposome, since in the Only-LPs treatment group, liposomes were observed up to approximately 60 μm distance from the blood vessel.

3.6. Therapeutic efficacy

A treatment study was performed to assess whether the improved delivery of liposomes by ultrasound could improve the therapeutic response. Tumours were treated with ultrasound of MI = 0.8 in the presence of microbubble as this treatment showed highest tumour uptake of liposomes. The relative tumour growth curves of individual animals treated with the Doxil-like, NonCleavable, Cleavable liposome and free doxorubicin are shown in Supplementary Fig. S8A–D, respectively. Animals that showed a reduced tumour growth with respect to the saline group for at least 7 consecutive days were defined as responders. Mice were euthanized when the tumour length exceeded 15 mm. The tumour growth, number of responders and median survival of the different treatment groups are summarized in Table 5. No significant

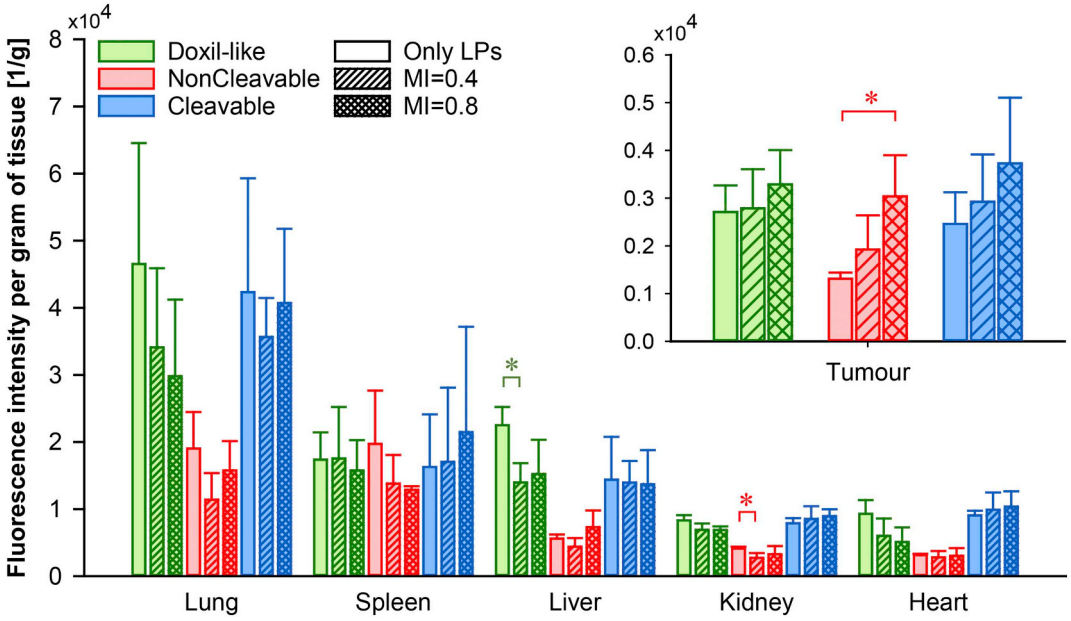

Fig. 4. Biodistribution in organs and tumours visualized as fluorescence intensity per gram of tissue for the three liposomes 3 hours post injection. Group means are shown, and error bars indicate the standard deviation. Statistical significance is shown with an asterisk. (*$p < 0.05$). Mean and standard deviation are based on 3–5 animals.

weight loss, which is a common side effect of cytostatic drugs, was observed for any of the treatments (see Supplementary Fig. S9).

Except for one animal in the control group, most control animals were euthanized between day 28 and 35. Therefore, the mean tumour growth for the first 28 days are shown in Fig. 6A. Solid lines indicate the Only-LPs or free drug treated groups, while the dashed lines indicate ultrasound treated groups. Comparing the control group (saline) with the Doxil-like + FUS, Cleavable + FUS and DOX + FUS treatment groups, a statistically significant reduction in tumour growth was found (58%, 39% and 21%, respectively). Surprisingly, the mice given the free drug had statistically larger tumours with respect to the control animals (+37%) at day 28. When comparing the Only-LPs or free drug treatment with the corresponding ultrasound treatment (-FUS vs +FUS), a statistically significant difference in tumour volume at day 28 was observed for the Doxil-like liposome and free drug treatment.

Of the Only-LPs and only free drug treatment groups, animals treated with the Doxil-like liposome showed the highest number of responders (4/7) followed by the Cleavable (2/5), NonCleavable (2/6) and Free Doxorubicin group (0/6). Using ultrasound and microbubbles in addition resulted in an increased number of responders in all treatment groups with again the highest number of responders for the Doxil-like liposome, i.e. 4 out of 5 of which 2 survived until the end of the study (100 days after first treatment) of which 1 was in full remission. The number of responders for the Cleavable, NonCleavable and Free doxorubicin treatment group increased to 4/6, 4/6 and 3/7, respectively.

The Kaplan-Meier plot in Fig. 6B represents the survival of the animals. Ultrasound and microbubbles combined with injection of the liposomes or free drug, resulted in a prolonged median survival but to different extents. Doxil-like + FUS (51 days, $p = 0.003$), Cleavable + FUS (40.5 days, $p = 0.029$) and DOX + FUS (42 days, $p = 0.037$) resulted in a significantly prolonged survival compared to the control group (32 days, saline). Of the Only-LPs treatment groups, only the Doxil-like liposome resulted in statistically significant increase (39 days, $p = 0.05$) in survival with respect to the control group (32 days, saline). In case of Doxil-like liposomes, there was a borderline significance between the Only-LPs and ultrasound treatment group ($p = 0.055$).

4. Discussion

4.1. Cellular uptake and cytotoxicity

Successful therapeutic response requires efficient cellular uptake and cytotoxicity of the drug-loaded liposomes. The three liposomes were taken up by the cells to various degrees, where NonCleavable performed best, followed by the Cleavable and Doxil-like liposome. The cytotoxicity study showed that both the encapsulated and free drug reduced cell viability, demonstrating the sensitivity of the PC3 cell line to the drug.

Both cellular uptake and cytotoxicity of the liposomes depend on cell-liposome interactions which are based on liposome properties like size and charge [33]. The liposomes used showed only minimal differences in size and charge which therefore cannot fully explain the results obtained. A possible explanation for the obtained differences in cellular uptake and cytotoxicity can be the differences in lipid compositions of the liposomal formulations. Both the Cleavable and NonCleavable liposomes contain unsaturated lipids which have reduced alignment due to the tail being kinked and thereby pack less tightly whilst saturated lipid tails can readily align and pack tightly. The reduced alignment of the unsaturated lipid tails leads to unsaturated bilayers having less rigidity than saturated bilayers (Doxil-like) leading to a faster rate of drug release [34]. This could have caused higher cellular doxorubicin fluorescence compared to the Doxil-like liposome as well as similar cytotoxicity profiles of the NonCleavable and Cleavable liposomes and the free drug.

Enzymatic removal of PEG increased the cellular uptake of the Cleavable liposomes compared to Cleavable liposomes treated with the same activation buffer without thermolysin, demonstrating that the PEG layer can prevent cellular uptake which has also been reported by others [28,29]. Thermolysin had no effect on the cellular uptake of the NonCleavable or Doxil-like liposomes, showing that the thermolysin specifically cleaved the PEGylated cleavable lipopeptide. Incubating PC3 cells with either the NonCleavable or Cleavable liposome in growth medium containing the enzyme activation buffer without thermolysin resulted in a reduced cellular uptake which indicates that adding the enzyme activation buffer to the growth medium potentially changed the metabolic activity and/or cellular uptake mechanisms of the PC3 cells. Most likely due to dilution of the growth medium or the composition of the enzyme activation buffer.

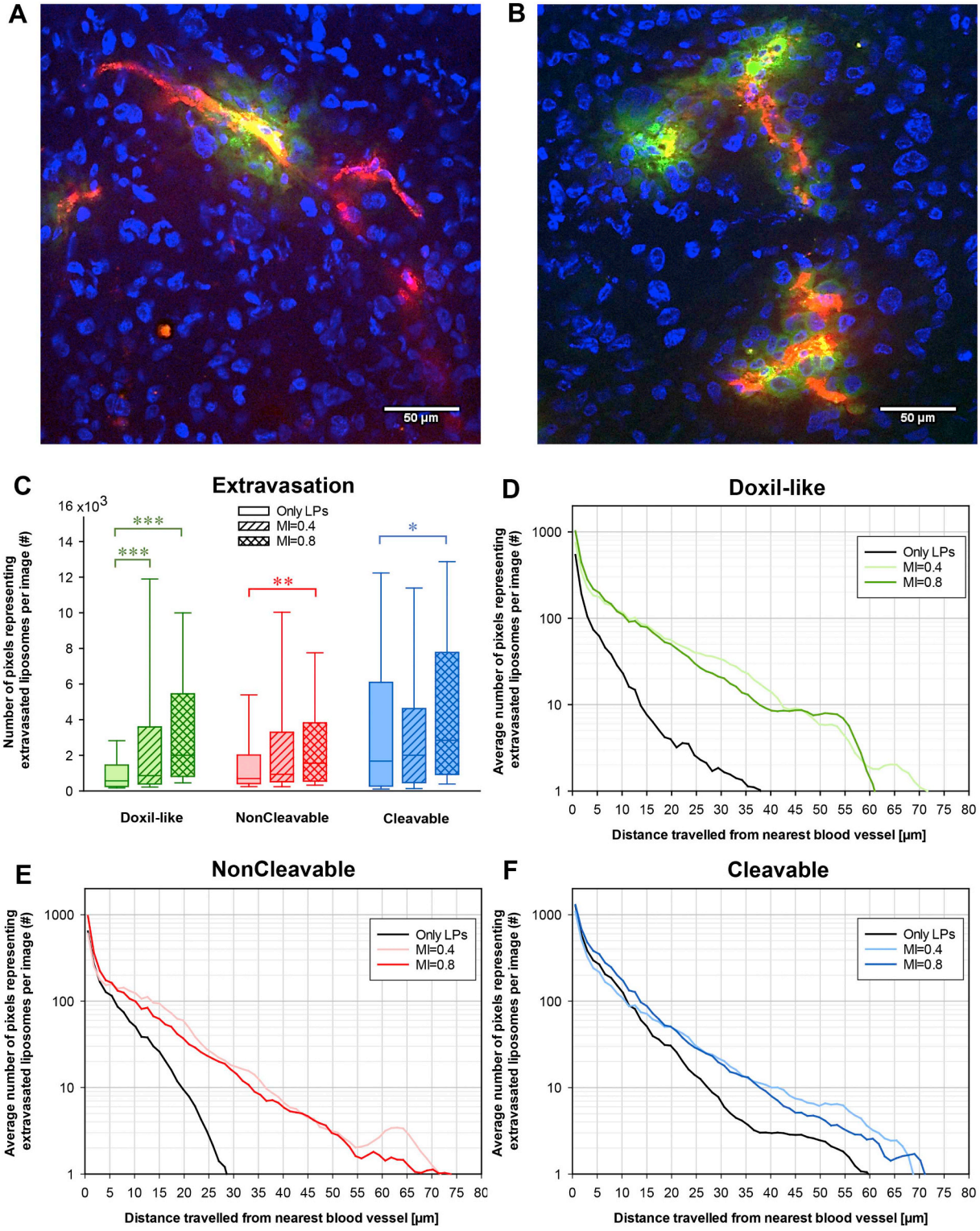

Fig. 5. Representative images of animals treated with (A) only LPs and (B) LPs in combination with MI = 0.8 ultrasound and microbubbles. LPs are shown in green, blood vessels in red and cell nuclei in blue. Scale bar is 50 µm. (C) The average number of pixels representing extravasated liposomes per image per treatment group and liposome. Results are based on 80 to 110 images per treatment group. Solid line in the boxplot and error bars represent the median and standard deviation, respectively. Statistically significance is shown with an asterisk (*$p < 0.05$, **$p < 0.01$, ***$p < 0.001$) (D-F) The average number of liposomes as a function of the distance travelled from the blood vessels, for the Doxil-like, NonCleavable and Cleavable liposomes, respectively.

4.2. Effect of ultrasound and microbubbles on the tumour accumulation of liposomes

Ultrasound in the presence of microbubbles resulted in a significant increase in accumulation of all three liposomes in tumours compared to the Only-LPs treatment groups. The Doxil-like and Cleavable liposome showed similar relative accumulation kinetics, while the NonCleavable liposome showed higher accumulation. 3 hours post treatment the NonCleavable liposome showed similar relative accumulation compared to the other two liposomes.

Table 5
The mean tumour volume at day 28, number of responders and median survival of the different treatment groups. Asterisks indicate statistical significance with respect to the saline group (D = Doxil-like, NC = NonCleavable, C = Cleavable, DOX = Free doxorubicin) (*p < 0.05, **p < 0.01, ***p < 0.001).

Treatment	Mean tumour volume at day 28 [mm^3]		Tumour volume w.r.t. saline at day 28 [%]		Nr. Responders		Median survival [Days]	
	−FUS	+FUS	−FUS	+FUS	−FUS	+FUS	−FUS	+FUS
Saline	888 ± 136	–	–	–	–	–	32	–
D	741 ± 403	372 ± 150 ***	−17%	−58%	4/7	4/5	39 *	51 **
NC	781 ± 98	701 ± 216	−12%	−21%	2/6	4/6	32.5	35
C	832 ± 93	539 ± 225 *	−6%	−39%	2/5	4/6	35	40.5 *
DOX	1236 ± 207 *	698 ± 117 *	+39%	−21%	0/6	3/7	31	42 *

The fluorescence in the tumour ROI will originate from both liposomes still in circulation and liposomes that have extravasated. Assuming that the ultrasound treatment does not change the circulation properties of the liposomes, the increase in relative fluorescence intensity can be attributed to sonopermeation effects.

Microbubbles are constrained to the blood vessels, and their *in* vivo behaviour depends on the ultrasound parameters (frequency, pressure, pulse duration, pulse repetition), microbubble properties (size, shell properties, concentration) and *in vivo* conditions like vessel diameter, vascular structure and viscosity of the blood [21,35–37]. Microbubbles exposed to ultrasound can undergo stable volumetric oscillations, also known as stable cavitation, or more radical oscillations resulting in a violent collapse of the bubble which is known as inertial cavitation. It has been shown that stable cavitation causes microstreaming, improves vascular permeability and stimulates endocytosis, and inertial cavitation might result in shock waves and microjets, which when close to a membrane, can result in transient or permanent pores in the vascular wall or even to more extensive vascular damage [20,23,38,39].

The effect of a wide range of ultrasound parameters on the cavitation behaviour of SonoVue^{TM} microbubbles has been studied mainly in an *in vitro* setting. Based on *in vitro* studies, inertial cavitation was observed above an MI of 0.5 [40,41], while *in vivo* inertial cavitation became observable at MI > 0.62 [41]. Thus, it is expected that in the case of the MI = 0.4 treatment groups mainly stable cavitation occurs and when using an MI of 0.8, more inertial cavitation is expected. This was confirmed when detecting the cavitation behaviour of SonoVue^{TM} (see Supplementary Fig. S10), both more stable and inertial cavitation was observed in the MI = 0.8 group compared to the MI = 0.4 group. The difference in microbubble behaviour and the corresponding biomechanical effects are likely to be the reason for the higher uptake of liposomes and improved extravasation in the MI = 0.8 groups.

Ultrasound in the presence of microbubbles can change the perfusion. Both vascular shutdown and increased perfusion by opening of non-perfused microvessels, have been reported [42,43]. An increased perfusion of the tumour could partly explain the observed increase in tumour fluorescence intensity in the ultrasound treatment groups.

If cavitation and perfusion do not differ between the three liposomes, the observed increased tumour uptake of the NonCleavable liposome with respect to the other two liposomes, should be due to an interplay of liposome properties (formulation, size, charge, PEGylation, etc.), tumour characteristics (vascularization, EPR-effect, etc.) and interaction with blood components. In both the NonCleavable and Cleavable liposome, cholesterol is used as the lipid anchor of the PEG. Cholesterol is known to partition out which could result in the liposomes losing their PEG-layer over time thereby altering their *in vivo* behaviour. That this happens cannot be completely ruled out, but it is expected that the effect will be minimal and similar across the NonCleavable and Cleavable liposome because of the similar amount of Chol-PEG used in both formulations. The size of the Cleavable and NonCleavable liposome did not differ while the Doxil-like liposome exhibited a slightly smaller size which can be beneficial with respect to extravasation. The NonCleavable liposome had a higher zeta potential (-3.8 mV) compared to the Doxil-like and Cleavable liposome (-13.4 mV and -13.7 mV, respectively) and it has been shown that a more neutral charge of the particles could result in less interactions with the negatively charged endothelial cell membrane and extracellular matrix components and thereby increase the extravasation and diffusion rate [26,44,45]. In addition, neutral liposomes show less interaction with charged blood components whereas more negatively or positively charged liposomes will undergo more and different protein adsorption

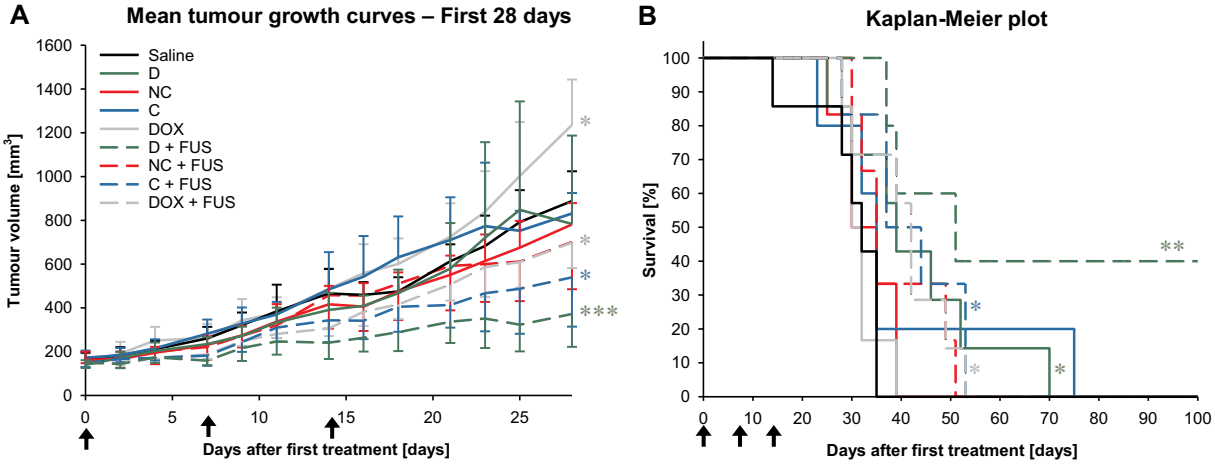

Fig. 6. (A) Tumour growth curves of the first 28 days after the first treatment. Line plot and error bars represent the mean of 5–7 mice and standard deviation, respectively. Asterisks show significant tumour reductions with respect to the saline treatment group (*p < 0.05, ***p < 0.001) (B) Kaplan-Meier plot. Different colours indicate the different LPs or drug used. Solid lines indicate only LPs or drug treatment groups. Dashed lines indicate the ultrasound treatment groups (+FUS). Treatments took place on day 0, 7 and 14 and are indicated with a black arrow. (*p < 0.05, **p < 0.01) (D = Doxil-like, NC = NonCleavable, C = Cleavable, DOX = Free doxorubicin, FUS = Focused ultrasound and microbubbles).

hence altering their properties, i.e. size, shape, charge, etc., which will affect their extravasation and tumour accumulation [46,47]. The more neutral charge of the NonCleavable liposome could therefore potentially have been beneficially for tumour accumulation rate.

4.3. Biodistribution of liposomes in tumour and normal organs

Imaging of the excised tumour showed increased tumour accumulation of the liposomes after ultrasound which is consistent with the *in vivo* measurements done 3 hours post treatment. However, most of the statistical significance between the Only-LPs and ultrasound treatment groups found in the *in vivo* dataset was lost after excising the tumour. This is most likely due to the correction for the weight of the tumour in the *ex vivo* biodistribution dataset.

The biodistribution of normal organs showed that ultrasound and microbubbles did not alter the biodistribution profiles of the organs. Organs were excised three hours after ultrasound treatment and based on the circulation half-life time of 3 to 4 hours (see Table S1 and Fig. S2), the measured fluorescence intensity will originate both from liposomes still in circulation and liposomal uptake by the organs. The relative high uptake by the lungs, especially for the Cleavable and Doxil-like liposome, is interesting. A possible explanation could be that the lung capillaries are the first capillaries the liposomes encounter after injection in the lateral tail vein such that aggregates get stuck in the microvasculature of the lungs. In addition, the lungs of mice have the largest mean blood volume per gram of wet tissue (0.49 ml) followed by liver (0.36 ml), kidneys (0.34 ml) and spleen (0.17 ml) which could be one of the reasons of the relatively high fluorescence intensity originating from the lungs for all three liposomes [48]. High fluorescence intensities of the spleen and liver are expected since macrophages, which are responsible for clearing liposomes and other substances from the blood, are residing in those organs [49].

4.4. Microdistribution – Extravasation and penetration depth of liposomes

After recording tumour accumulation of the liposomes, the intra tumoural microdistribution of the liposomes in frozen tumour tissues was imaged by CLSM. The Cleavable liposome was found to extravasate to a larger extent than the other two liposomes. For all liposomes, the exposure to ultrasound and microbubbles increased the extravasation significantly and most profoundly after MI = 0.8. Many have reported on enhanced extravasation of liposomes in tumours after exposure to ultrasound and microbubbles, which is most likely caused by cavitating microbubbles increasing the vascular permeability in the tumour [11–15]. Here an MI of 0.4 and 0.8 were used, and improved extravasation was observed for increasing MI and for both ultrasound treatment groups with respect to the Only-LPs group, which agrees well with what have been reported [13,37].

Physiochemical properties and tumour characteristics will determine the *in vivo* fate of the liposomes including their extravasation and tumour penetration [9,50,51]. When no ultrasound is used, penetration of liposomes through the extracellular matrix will be mainly diffusion driven due to the high interstitial fluid pressure, which favours the use of liposomes with a smaller hydrodynamic diameter [52,53]. Interestingly, the Cleavable liposome showed almost a doubled penetration depth with respect to the other two liposomes when no ultrasound was used. A potential reason could be the enzyme sensitive properties of the liposome. The animals were euthanized 3 hours post treatment and within those 3 hours, the extravasated liposomes will come in contact with MMPs causing cleavage of the PEG layer. The presence and activity of the MMPs in the used tumour model has been shown by *in situ* zymography (see Supplementary Fig. S11). MMPs of interest are located at the basement membranes along collagen type IV fibres, thus PEG cleavage can take place immediately after extravasation [54]. How fast and to what extent the PEG layer will be cleaved will depend on several factors including liposome concentration, enzyme concentrations and accessibility of the peptide for the enzymes. PEG cleavage by MMPs reveals a negatively charged residue which could facilitate electrostatic interactions with the ECM, enhancing liposome retention.

Ultrasound increased the penetration of all liposomes into the ECM, and the effect was the smallest for the Cleavable liposome. Interestingly, even though the amount of extravasation was different for the three liposomes, the distance travelled from the nearest blood vessel was rather similar between the liposomes in the two ultrasound groups, and in accordance with penetration depths reported by others [55]. The observed improved penetration depth could indicate that sonopermeation also causes extravascular effects such as acoustic streaming, shockwave generation, jet formation and possible structural changes in the extracellular matrix and creation of pores [23,56]. Even though the microbubbles showed a clear increase in cavitation behaviour at the higher MI (Supplementary Fig. S10), surprisingly, a similar penetration depth was observed in the studied time window. Both our observations and reports from others might indicate that there is a maximum penetration depth of liposomes from the blood vessels [55].

4.5. Therapeutic efficacy study

The tumours exposed to the Doxil-like liposome combined with ultrasound and microbubbles showed the best therapeutic response. A tumour volume reduction up to ~60% with respect to the control group (saline) was obtained, the number of responders increased, and median survival was prolonged. Also for the Cleavable liposome and the free drug doxorubicin, an improved therapeutic response was observed after ultrasound-mediated delivery, but to a lower extent. The ultrasound treatments used are not expected to have any therapeutic effect on their own. This assumption is supported by studies in [57,58].

When comparing the observed microdistribution of the liposomes with the obtained therapeutic efficacy of the liposomes, it should be kept in mind that both experiments have been performed with different batches of liposomes. For each of the liposomes, the variability in size and zeta potential between the different batches used for both the *in vitro* and *in vivo* experiments are small and within acceptable values, but could indicate for example differences in PEG coverages. This could have affected the *in vivo* behaviour of the liposomes, also with respect to the observed *in vitro* behaviour. Due to the relatively small differences in zeta potential and size between the different batches used, a large impact on the *in vivo* behaviour of the liposomes is not expected, but small alterations in *in vivo* behaviour cannot be ruled out. Due to the expected minor effect, it is assumed that the obtained microdistribution data is representative for the *in vivo* behaviour of the liposomes when discussing the therapeutic efficacy.

Even though the Cleavable liposome already extravasated and penetrated the extracellular matrix well by itself compared to the other two liposomes, no effect on the therapeutic efficacy of the Only-LPs treatment was observed. One possible explanation could be that although many liposomes penetrated far into the extracellular matrix, the number was not sufficient for any therapeutic effect. It is possible that cleaving of the PEG increased the uptake of the liposomes by macrophages and other non-tumour cells. The majority of nanoparticles is reported to either being trapped in the extracellular matrix or taken up by perivascular cells and other macrophages resulting in 0.0014% of administered nanoparticles being internalized by the tumour cells [59]. So even though the Cleavable liposome seemed to extravasate the best of the three liposomes, the final number reaching the tumour cells was not sufficient for any therapeutic effect. Adding ultrasound and microbubbles to the treatment resulted in an improved extravasation of the Cleavable liposome, but the penetration depth was only minimally affected. This reduced the tumour growth with almost a factor 6.5 (39%/6%) 28 days after the first treatment.

The difference in therapeutic efficacy between the NonCleavable and Cleavable liposome is interesting since the differences in liposome

properties (lipid formulation, size, charge) were minimal. Nevertheless, the Cleavable liposome extravasated and penetrated the extracellular matrix better than the NonCleavable liposome. Even though the extravasation and penetration of the NonCleavable liposome was similar to the successful Doxil-like liposome and the number of responders was similar to the Cleavable liposome, no effect on therapeutic efficacy was observed. This could indicate that the MMP sensitive property of the Cleavable liposome has positively affected the therapeutic efficacy as well.

Interestingly, the group of animals receiving only free doxorubicin showed increased tumour growth with respect to the control group. It has been reported that low doses of doxorubicin can induce drug resistance which could explain the observed induced tumour growth [60]. In case of the ultrasound treatment group, the animals showed a significant reduced tumour growth, which is interesting since the drug molecule should be able to diffuse easily by itself into the tumour tissue. Nevertheless, sonopermeation potentially resulted in an increased local delivery to tumour tissue such that free doxorubicin became more efficient. Improved ultrasound-mediated therapeutic response of small drugs has also been observed in a clinical trial on inoperable pancreatic cancer [17].

The promising preclinical studies demonstrating that ultrasound and microbubbles improve delivery of nanomedicine and enhance the therapeutic response, have led to several clinical studies ([17], NCT03477019, NCT00245869 and more). When using ultrasound-mediated delivery of drugs and liposomes in the clinic, stratification of patients to determine which patients will benefit from the treatment is important. It has been shown preclinically that tumours with low EPR effect, such as the PC3 tumour model used in the present study, benefits more from the use of ultrasound-mediated delivery of liposomes compared to tumours that are well vascularized and have a high EPR effect [55].

The current study showed that combined with ultrasound and microbubbles, the Cleavable liposome had a better therapeutic efficacy compared to the NonCleavable liposome indicating that cleaving of the PEG-layer can be important. However, the Doxil-like liposome outcompeted the NonCleavable and Cleavable liposomes and free drug doxorubicin treatment groups both with and without the use of ultrasound and microbubbles.

5. Conclusion

Focused ultrasound in the presence of microbubbles resulted in an improved tumour accumulation, increased extravasation and increased penetration depth of liposomes into the extracellular matrix compared to mice receiving just an injection of liposomes. The Cleavable liposome performed better than the NonCleavable both in terms of extravasation, microdistribution and therapeutic efficacy. Both for Doxil-like and Cleavable liposomes, the ultrasound-mediated delivery resulted in an improved therapeutic efficacy.

Declaration of Competing Interest

The authors declare that they have no known competing financial interests or personal relationships that could have appeared to influence the work reported in this paper.

Acknowledgements

Kristin Grendstad from NTNU is thanked for technical assistance with cell culturing and flow cytometry. Lars Ringgaard Petersen and Gael Clergeaud Veiga from DTU are acknowledged for their technical support. Housing of the animals was provided by the Comparative Medicine Core Facility (CoMed, NTNU). Tissue sections were prepared by the Cellular and Molecular Imaging Core Facility (CMIC, NTNU). Astrid Bjørkøy and the Centre for Molecular Imaging at the Faculty of Natural Sciences (MINT, NTNU) are thanked for technical assistance with CLSM. The project was internally funded by the Norwegian University of Science and Technology (NTNU, Trondheim, Norway). Additional funding from the Central Norway Regional Health Authorities and the Norwegian Research Council (project 262228) is acknowledged.

Appendix A. Supplementary data

Supplementary data to this article can be found online at https://doi.org/10.1016/j.jconrel.2020.06.024.

References

[1] A.A. Epenetos, D. Snook, H. Durbin, P.M. Johnson, J. Taylor-Papadimitriou, Limitations of radiolabeled monoclonal antibodies for localization of human neoplasms, Cancer Res. 46 (1986) 3183–3191.
[2] H.-P. Gerber, P.D. Senter, I.S. Grewal, Antibody drug-conjugates targeting the tumor vasculature: current and future developments, MAbs, Taylor & Francis, 2009, pp. 247–253.
[3] A.K. Iyer, G. Khaled, J. Fang, H. Maeda, Exploiting the enhanced permeability and retention effect for tumor targeting, Drug Discov. Today 11 (2006) 812–818.
[4] H. Maeda, J. Wu, T. Sawa, Y. Matsumura, K. Hori, Tumor vascular permeability and the EPR effect in macromolecular therapeutics: a review, J. Control. Release 65 (2000) 271–284.
[5] J. Fang, H. Nakamura, H. Maeda, The EPR effect: unique features of tumor blood vessels for drug delivery, factors involved, and limitations and augmentation of the effect, Adv. Drug Deliv. Rev. 63 (2011) 136–151.
[6] D. Peer, J.M. Karp, S. Hong, O.C. Farokhzad, R. Margalit, R. Langer, Nanocarriers as an emerging platform for cancer therapy, Nat Nano 2 (2007) 751–760.
[7] S. Torosean, B. Flynn, J. Axelsson, J. Gunn, K.S. Samkoe, T. Hasan, M.M. Doyley, B.W. Pogue, Nanoparticle uptake in tumors is mediated by the interplay of vascular and collagen density with interstitial pressure, Nanomedicine: Nanotechnology, Biol. Med. 9 (2013) 151–158.
[8] A.A. Manzoor, L.H. Lindner, C.D. Landon, J.-Y. Park, A.J. Simnick, M.R. Dreher, S. Das, G. Hanna, W. Park, A. Chilkoti, Overcoming limitations in nanoparticle drug delivery: triggered, intravascular release to improve drug penetration into tumors, Cancer Res. 72 (2012) 5566–5575.
[9] R.K. Jain, T. Stylianopoulos, Delivering nanomedicine to solid tumors, Nat. Rev. Clin. Oncol. 7 (2010) 653–664.
[10] L. Eikenes, I. Tufto, E.A. Schnell, A. Bjørkøy, C.D.L. Davies, Effect of collagenase and hyaluronidase on free and anomalous diffusion in multicellular spheroids and xenografts, Anticancer Res. 30 (2010) 359–368.
[11] S. Eggen, M. Afadzi, E.A. Nilssen, S.B. Haugstad, B. Angelsen, C.D.L. Davies, Ultrasound improves the uptake and distribution of liposomal Doxorubicin in prostate cancer xenografts, Ultrasound Med. Biol. 39 (2013) 1255–1266.
[12] S. Eggen, S.-M. Fagerland, Ý. Mørch, R. Hansen, K. Søvik, S. Berg, H. Furu, A.D. Bøhn, M.B. Lilledahl, A. Angelsen, Ultrasound-enhanced drug delivery in prostate cancer xenografts by nanoparticles stabilizing microbubbles, J. Control. Release 187 (2014) 39–49.
[13] S. Snipstad, S. Berg, Ý. Mørch, A. Bjørkøy, E. Sulheim, R. Hansen, I. Grimstad, A. van Wamel, A.F. Maaland, S.H. Torp, Ultrasound improves the delivery and therapeutic effect of nanoparticle-stabilized microbubbles in breast cancer xenografts, Ultrasound Med. Biol. 43 (2017) 2651–2669.
[14] S. Kotopoulis, A. Delalande, M. Popa, V. Mamaeva, G. Dimcevski, O.H. Gilja, M. Postema, B.T. Gjertsen, E. McCormack, Sonoporation-enhanced chemotherapy significantly reduces primary tumour burden in an orthotopic pancreatic cancer xenograft, Mol. Imag. Biol. 16 (2014) 53–62.
[15] C.-Y. Lin, J.-R. Li, H.-C. Tseng, M.-F. Wu, W.-L. Lin, Enhancement of focused ultrasound with microbubbles on the treatments of anticancer nanodrug in mouse tumors, Nanomedicine: Nanotechnology, Biol. Med. 8 (2012) 900–907.
[16] M. Aryal, N. Vykhodtseva, Y.-Z. Zhang, J. Park, N. McDannold, Multiple treatments with liposomal doxorubicin and ultrasound-induced disruption of blood–tumor and blood–brain barriers improve outcomes in a rat glioma model, J. Control. Release 169 (2013) 103–111.
[17] G. Dimcevski, S. Kotopoulis, T. Bjånes, D. Hoem, J. Schjøtt, B.T. Gjertsen, M. Biermann, A. Molven, H. Sorbye, E. McCormack, A human clinical trial using ultrasound and microbubbles to enhance gemcitabine treatment of inoperable pancreatic cancer, J. Control. Release 243 (2016) 172–181.
[18] A. Carpentier, M. Canney, A. Vignot, V. Reina, K. Beccaria, C. Horodyckid, C. Karachi, D. Leclercq, C. Lafon, J.Y. Chapelon, Clinical trial of blood-brain barrier disruption by pulsed ultrasound, Sci. Transl. Med. 8 (2016) 343re342-343re342.
[19] I. De Cock, E. Zagato, K. Braeckmans, Y. Luan, N. de Jong, S.C. De Smedt, I. Lentacker, Ultrasound and microbubble mediated drug delivery: acoustic pressure as determinant for uptake via membrane pores or endocytosis, J. Control. Release 197 (2015) 20–28.
[20] I. Lentacker, I. De Cock, R. Deckers, S. De Smedt, C. Moonen, Understanding ultrasound induced sonoporation: definitions and underlying mechanisms, Adv. Drug Deliv. Rev. 72 (2014) 49–64.
[21] K. Kooiman, H.J. Vos, M. Versluis, N. de Jong, Acoustic behavior of microbubbles

and implications for drug delivery, Adv. Drug Deliv. Rev. 72 (2014) 28–48.
[22] M. Afadzi, S.P. Strand, E.A. Nilssen, S.-E. Masøy, T.F. Johansen, R. Hansen, B.A. Angelsen, C.D.L. Davies, Mechanisms of the ultrasound-mediated intracellular delivery of liposomes and dextrans, IEEE Trans. Ultrason. Ferroelectr. Frequency Control 60 (2012) 21–33.
[23] S. Snipstad, E. Sulheim, C. de Lange Davies, C. Moonen, G. Storm, F. Kiessling, R. Schmid, T. Lammers, Sonopermeation to improve drug delivery to tumors: from fundamental understanding to clinical translation, Exp. Opin. Drug Deliv. 15 (2018) 1249–1261.
[24] A. Gabizon, F. Martin, Polyethylene glycol-coated (pegylated) liposomal doxorubicin, Drugs 54 (1997) 15–21.
[25] M.J. Ernsting, M. Murakami, A. Roy, S.-D. Li, Factors controlling the pharmacokinetics, biodistribution and intratumoral penetration of nanoparticles, J. Control. Release 172 (2013) 782–794.
[26] T. Stylianopoulos, M.-Z. Poh, N. Insin, M.G. Bawendi, D. Fukumura, L.L. Munn, R.K. Jain, Diffusion of particles in the extracellular matrix: the effect of repulsive electrostatic interactions, Biophys. J. 99 (2010) 1342–1349.
[27] S. Lélu, S.P. Strand, J. Steine, C.D.L. Davies, Effect of PEGylation on the diffusion and stability of chitosan–DNA polyplexes in collagen gels, Biomacromolecules 12 (2011) 3656–3665.
[28] S. Mishra, P. Webster, M.E. Davis, PEGylation significantly affects cellular uptake and intracellular trafficking of non-viral gene delivery particles, Eur. J. Cell Biol. 83 (2004) 97–111.
[29] B. Romberg, W.E. Hennink, G. Storm, Sheddable coatings for long-circulating nanoparticles, Pharm. Res. 25 (2008) 55–71.
[30] M. Roomi, J. Monterrey, T. Kalinovsky, M. Rath, A. Niedzwiecki, Patterns of MMP-2 and MMP-9 expression in human cancer cell lines, Oncol. Rep. 21 (2009) 1323–1333.
[31] J. Bruun, T.B. Larsen, R.I. Jølck, R. Eliasen, R. Holm, T. Gjetting, T.L. Andresen, Investigation of enzyme-sensitive lipid nanoparticles for delivery of siRNA to blood-brain barrier and glioma cells, Int. J. Nanomed. 10 (2015) 5995–6008.
[32] S. Snipstad, S. Hak, H. Baghirov, E. Sulheim, Ý. Mørch, S. Lélu, E. von Haartman, M. Bäck, K.P.R. Nilsson, A.S. Klymchenko, Labeling nanoparticles: Dye leakage and altered cellular uptake, Cytometry Part A 91 (2017) 760–766.
[33] A. Verma, F. Stellacci, Effect of surface properties on nanoparticle–cell interactions, Small 6 (2010) 12–21.
[34] T. Lian, R.J. Ho, Trends and developments in liposome drug delivery systems, J. Pharm. Sci. 90 (2001) 667–680.
[35] N. Hosseinkhah, K. Hynynen, A three-dimensional model of an ultrasound contrast agent gas bubble and its mechanical effects on microvessels, Phys. Med. Biol. 57 (2012) 785–808.
[36] X. Guo, Q. Li, Z. Zhang, D. Zhang, J. Tu, Investigation on the inertial cavitation threshold and shell properties of commercialized ultrasound contrast agent microbubbles, J. Acoust. Soc. Am. 134 (2013) 1622–1631.
[37] P.T. Yemane, A.K. Åslund, S. Snipstad, A. Bjørkøy, K. Grendstad, S. Berg, Y. Mørch, S.H. Torp, R. Hansen, C. de Lange Davies, Effect of Ultrasound on the Vasculature and Extravasation of Nanoscale Particles Imaged in Real Time, Ultrasound Med. Biol. 45 (2019) 3028–3041.
[38] V. Frenkel, Ultrasound-mediated delivery of drugs and genes to solid tumors, Adv. Drug Deliv. Rev. 60 (2008) 1193–1208.
[39] Y. Hu, J.M. Wan, C. Alfred, Membrane perforation and recovery dynamics in microbubble-mediated sonoporation, Ultrasound Med. Biol. 39 (2013) 2393–2405.
[40] Y. Lin, L. Lin, M. Cheng, L. Jin, L. Du, T. Han, L. Xu, C. Alfred, P. Qin, Effect of acoustic parameters on the cavitation behavior of SonoVue microbubbles induced by pulsed ultrasound, Ultrason. Sonochem. 35 (2017) 176–184.
[41] S.-K. Wu, P.-C. Chu, W.-Y. Chai, S.-T. Kang, C.-H. Tsai, C.-H. Fan, C.-K. Yeh, H.-L. Liu, Characterization of different microbubbles in assisting focused ultrasound-induced blood-brain barrier opening, Sci. Rep. 7 (2017) 46689.
[42] C.P. Keravnou, I. De Cock, I. Lentacker, M.-L. Izamis, M.A. Averkiou, Microvascular injury and perfusion changes induced by ultrasound and microbubbles in a machine-perfused pig liver, Ultrasound Med. Biol. 42 (2016) 2676–2686.
[43] X. Hu, A. Kheirolomoom, L.M. Mahakian, J.R. Beegle, D.E. Kruse, K.S. Lam, K.W. Ferrara, Insonation of targeted microbubbles produces regions of reduced blood flow within tumor vasculature, Invest. Radiol. 47 (2012) 398.
[44] S. Krasnici, A. Werner, M.E. Eichhorn, M. Schmitt-Sody, S.A. Pahernik, B. Sauer, B. Schulze, M. Teifel, U. Michaelis, K. Naujoks, Effect of the surface charge of liposomes on their uptake by angiogenic tumor vessels, Int. J. Cancer 105 (2003) 561–567.
[45] O. Lieleg, R.M. Baumgärtel, A.R. Bausch, Selective filtering of particles by the extracellular matrix: an electrostatic bandpass, Biophys. J. 97 (2009) 1569–1577.
[46] J. Lazarovits, Y.Y. Chen, E.A. Sykes, W.C. Chan, Nanoparticle–blood interactions: the implications on solid tumour targeting, Chem. Commun. 51 (2015) 2756–2767.
[47] S.M. Ahsan, C.M. Rao, M.F. Ahmad, Nanoparticle-protein interaction: the significance and role of protein corona, Cellular and Molecular Toxicology of Nanoparticles, Springer, 2018, pp. 175–198.
[48] N. Kaliss, D. Pressman, Plasma and blood volumes of mouse organs, as determined with radioactive iodoproteins, Proc. Soc. Exp. Biol. Med. 75 (1950) 16–20.
[49] S.-D. Li, L. Huang, Pharmacokinetics and biodistribution of nanoparticles, Mol. Pharm. 5 (2008) 496–504.
[50] Q. Sun, T. Ojha, F. Kiessling, T. Lammers, Y. Shi, Enhancing tumor penetration of nanomedicines, Biomacromolecules 18 (2017) 1449–1459.
[51] Y.R. Zhang, R. Lin, H.J. Li, W.L. He, J.Z. Du, J. Wang, Strategies to improve tumor penetration of nanomedicines through nanoparticle design, Wiley Interdiscip. Rev. Nanomed. Nanobiotechnol. 11 (2019) 1519.
[52] R.K. Jain, L.T. Baxter, Mechanisms of heterogeneous distribution of monoclonal antibodies and other macromolecules in tumors: significance of elevated interstitial pressure, Cancer Res. 48 (1988) 7022–7032.
[53] H. Cabral, Y. Matsumoto, K. Mizuno, Q. Chen, M. Murakami, M. Kimura, Y. Terada, M. Kano, K. Miyazono, M. Uesaka, Accumulation of sub-100 nm polymeric micelles in poorly permeable tumours depends on size, Nat. Nanotechnol. 6 (2011) 815.
[54] O.R. Mook, C.V. Overbeek, E.G. Ackema, F.V. Maldegem, W.M. Frederiks, In situ localization of gelatinolytic activity in the extracellular matrix of metastases of colon cancer in rat liver using quenched fluorogenic DQ-gelatin, J. Histochem. Cytochem. 51 (2003) 821–829.
[55] B. Theek, M. Baues, T. Ojha, D. Möckel, S.K. Veettil, J. Steitz, L. van Bloois, G. Storm, F. Kiessling, T. Lammers, Sonoporation enhances liposome accumulation and penetration in tumors with low EPR, J. Control. Release 231 (2016) 77–85.
[56] S. Lee, H. Han, H. Koo, J.H. Na, H.Y. Yoon, K.E. Lee, H. Lee, H. Kim, I.C. Kwon, K. Kim, Extracellular matrix remodeling in vivo for enhancing tumor-targeting efficiency of nanoparticle drug carriers using the pulsed high intensity focused ultrasound, J. Control. Release 263 (2017) 68–78.
[57] R. Carlisle, J. Choi, M. Bazan-Peregrino, R. Laga, V. Subr, L. Kostka, K. Ulbrich, C.-C. Coussios, L.W. Seymour, Enhanced Tumor Uptake and Penetration of Virotherapy Using Polymer Stealthing and Focused Ultrasound, JNCI: J. Nat. Cancer Inst. 105 (2013) 1701–1710.
[58] A. van Wamel, P.C. Sontum, A. Healey, S. Kvåle, N. Bush, J. Bamber, C. de Lange Davies, Acoustic Cluster Therapy (ACT) enhances the therapeutic efficacy of paclitaxel and Abraxane® for treatment of human prostate adenocarcinoma in mice, J. Control. Release 236 (2016) 15–21.
[59] Q. Dai, S. Wilhelm, D. Ding, A.M. Syed, S. Sindhwani, Y. Zhang, Y.Y. Chen, P. MacMillan, W.C. Chan, Quantifying the ligand-coated nanoparticle delivery to cancer cells in solid tumors, ACS Nano 12 (2018) 8423–8435.
[60] C. Christowitz, T. Davis, A. Isaacs, G. Van Niekerk, S. Hattingh, A.-M. Engelbrecht, Mechanisms of doxorubicin-induced drug resistance and drug resistant tumour growth in a murine breast tumour model, BMC cancer 19 (2019) 757.